Rutting Prediction of Flexible Pavements Using Finite Element Modeling

Loay Akram Al-Khateeb [1], Andrews Saoud [2] and Mohammad Fawaz Al-Msouti [3]

[1] Department of Transport and Communication, Faculty of civil Engineering, Damascus University,
lokh73@yahoo.com
[2] Department of Transport and Communication, Faculty of Civil Engineering, Damascus University,
a-saoud@scs-net.org
[3] Department of Transport and Communication, Faculty of Civil Engineering, Damascus University,
f-msuti@scs-net.org

ABSTRACT

During the past two decades, Finite Element (FE) techniques were successfully used to simulate different pavement problems that could not be modelled using the simpler multi-layer elastic theory.

In this study, a two-dimensional finite element model was developed, using ABAQUS software, in order to investigate the impact of static repeated wheel load on rutting formation and pavement response. The procedures of building a model and performing static analysis are introduced. In that model, pavement materials were presented as linear-elastic–plastic based on Drucker-Prager model. In addition, the asphalt layer was assumed to follow a viscoelastic behavior using Pellinen and Witczak model, which was adopted by NCHRP. The Falling Weight Deflectometer FWD was also proposed as an effective and practical tool for on-site pavement evaluation and field measurements, other than the laboratory tests.

After insuring the model validation, the study investigated the impact of temperature, tire pressure and subgrade strength on the rut depth as a pavement response. The sensitivity analysis indicated that the rut depth increases with increasing the temperature and the tire pressure and with decreasing the subgrade strength.

KEYWORDS: Flexible pavement, Finite Element Method (FEM), Rutting, Falling Weight Deflectometer (FWD), ABAQUS program.

INTRODUCTION

Rutting is a main distress encountered in asphalt pavements, especially when the temperature is high as in a Syrian climate during the summer months. Rutting is caused by the accumulation of permanent deformation in all pavement layers under the action of repeated traffic loading. Among the contributions of rut depth by the various pavement layers, the cumulative permanent deformation in the surface course of asphalt pavement is known to be responsible for a major portion of the final rut depth measured on the pavement surface. So, rutting occurs only on flexible pavements, as indicated by the permanent deformation or rut depth along the wheel paths. The width and depth of the rut are widely affected by structural characters of the pavement layers (thickness and material quality), traffic loads and environmental conditions.

The objective of this research is to establish reliable rutting prediction models for an existing pavement. The

effects of temperature, subgrade properties and traffic loads on depth and development of the rutting as well as its relation with vertical plastic strain in the pavement and subgrade are also studied in the Syrian conditions. The numerical analysis of the model is based on the finite element method. The pavement structure analysis is performed using ABAQUS software package (Hibbitt, Karlsson and Sorensen). The results of the model analysis are calibrated with the field-measurements for the pavement of an arterial rural road

in the Syrian road network.

The importance of this research arises from the fact that several agencies adopted the rutting as a failure criterion in the pavement design. Almost all of these methods assumed a relation between the stress - strain and the following response of the pavement structure. The critical case is the stress and strain at the vertical axis of the center of the load, calculated at this point as shown in the Figure 1.
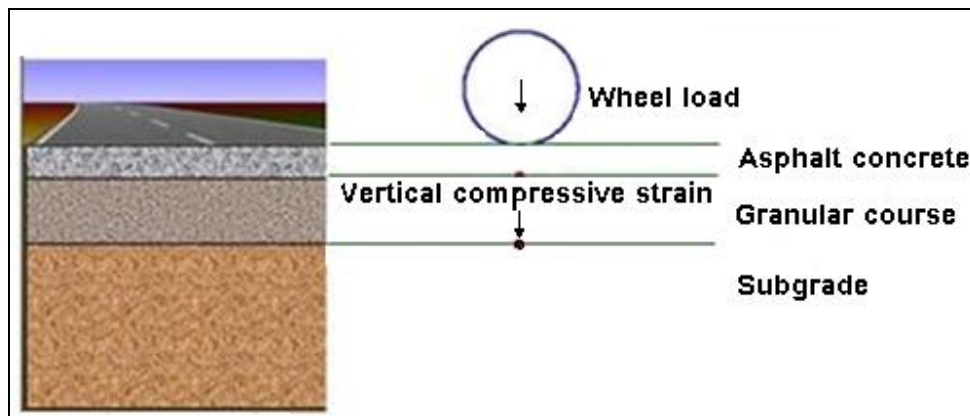

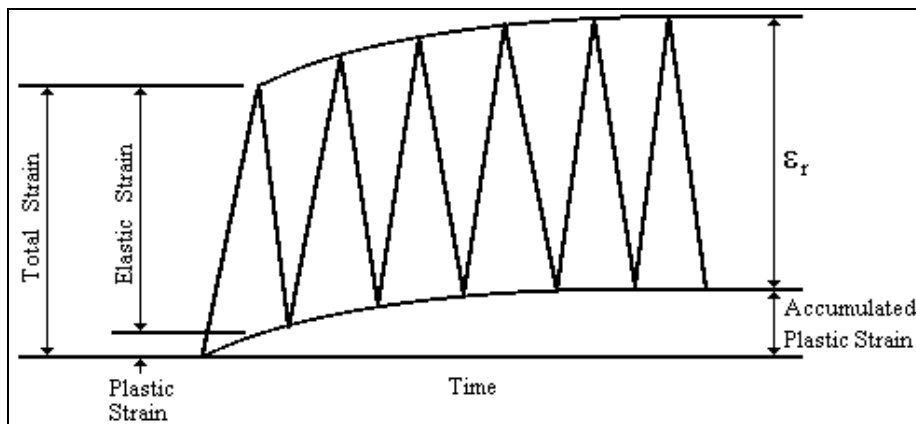**Figure 1: Pavement design due to rutting criterion**

Figure 2: Strains under repeated load

Dormon was the first researcher who suggested this design criterion in 1962 (Dormon, 1962). The flexible pavement layers are presented as a three layer structure of linear elastic materials subjected to a circular, uniformly distributed load. This classical design

criterion and compressive strain at the subgrade which occurs in high temperature conditions, were derived from Dormon's paper. The remarkable feature of this criterion is that it has remained the basis for mechanistic design.
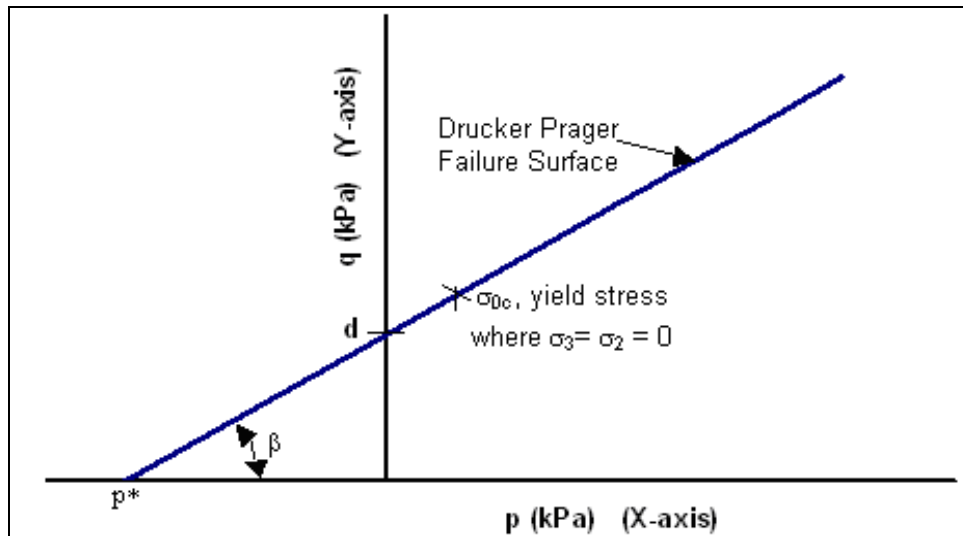
Figure 3: Drucker-Prager yield condition in 2D *p-q* stress space

The use of vertical compressive strain to control permanent deformation is based on the fact that plastic strains are proportional to elastic strains in paving materials. Thus, by limiting the elastic strains on the subgrade, the elastic strains in other components above the subgrade will also be controlled; hence, the magnitude of permanent deformation on the pavement surface will in turn be controlled (Huang, 2004).

Permanent Deformation

Another important observation is the fact that most paving materials experience some permanent deformation after each load application. Figure 2 shows how the amount of strain under repeated loading in a material changes over time. In the beginning, the material shows a considerable increase in the amount of permanent deformation (accumulated plastic strain). However, as the number of loads increases, the accumulated plastic strain levels off and the material is essentially elastic (recoverable strain). This phenomenon usually occurs after 100 to 200 load applications (Dormon, 1962).

For many years, it has been common practice to associate permanent deformation to excessive vertical strain on the top of the subgrade. It was assumed that if the pavement was well designed and the quality of pavement materials above the subgrade were well controlled, rutting could be reduced to tolerable levels by limiting the vertical strain on the subgrade. This approach minored the historic design approach for flexible pavements by assuming that structural design was merely a procedure to decrease stress in the controlling subgrade layer. Nevertheless, with time and enhanced technical capabilities and knowledge, it became quite clear that the total permanent deformation was a product of cumulative ruts occurring in all layers of the pavement system. The overall permanent deformation for a given season is the sum of permanent deformation for each individual layer and is mathematically expressed as: (NCHRP, 2004)

$$RD = \sum_{1}^{n} \varepsilon_p^i \ h^i \tag{1}$$

where:

RD: Pavement permanent deformation.
n : Number of the layers.
ε_p^i : Total plastic strain in the layer i.
h^i: Thickness of layer i.

PERFORMANCE OF MATERIALS

Viscoelastic Performance

The analytical design of flexible pavements requires that two aspects of material properties are examined. Firstly, the stress-strain characteristics, which are used to analyze critical stresses and strains in the structure. Secondly, the performance characteristics of the materials themselves which determine the deformation and likely the mode of failure (Shell, 1991). In recognition of these deformation patterns, various terms are in use to characterize the stress-strain relationships of pavement materials. Thus, the term used for asphalt mix performance is *viscoelastic*, including the determination of the dynamic modulus E^*. The National Cooperative Highway Research Program (NCHRP)

Project 1-37A recommends the use of the complex modulus as a design parameter in mechanistic design (Clyne et al., 2003). The dynamic modulus is the absolute value of the complex modulus, and is basically an elastic modulus obtained from a viscoelastic model which incorporates factors such as temperature, loading rate, bitumen viscosity and grain-size characteristics of the mix, among others. Pellinen and Witczak (2002) studied the behavior of 205 asphalt mixes and 23 binders in a temperature range between -18ºC and 54ºC with a loading frequency range of 0.1 to 25 Hz. They developed a predictive model to calculate the dynamic modulus. According to García and Thompson (2005), this model gives accurate results compared with laboratory results. The model is as follows (Pellinen and Witczak, 2002):

$$\log\left|E^*\right| = -1.249937 + 0.029232 P_{200} - 0.00176\,(P_{200})^2 + 0.002841 P_4 - 0.058097\,V_a - $$

$$0.802208\,\frac{V_{beff}}{(V_{beff} + V_a)} + \frac{\left[3.871977 - 0.0021 P_4 + 0.003958 P_{3/8} - 0.000017(P_{3/8})^2 + 0.00547 P_{3/4}\right]}{1 + e^{\left[-0.603313 - 0.313351\log(f) - 0.393532\log(\eta)\right]}} \tag{2}$$

where:

$|E^*|$ = asphalt mix complex modulus, in 10^5 psi;

f = load frequency, in Hz; $f = 1/t$, t = time loading, in sec;

V_a = percent air voids in the mix, by volume;

V_{beff} = percent effective bitumen content, by volume;

$P_{3/4}$ = percent retained on ¾-in. sieve, by total aggregate weight (cumulative);

$P_{3/8}$ = percent retained on 3/8-in. sieve, by total aggregate weight (cumulative);

P_4 = percent retained on No. 4 sieve, by total aggregate weight (cumulative);

P_{200} = percent passing No. 200 sieve, by total aggregate weight;

η = bitumen viscosity, in 10^6 poise.

Penetration data can be converted to viscosity using the following equation (NCHRP, 2004):

$\log \eta = 10.5012 - 2.2601 \log(Pen) + 0.00389 \log(Pen)^2$ (3)

where:

η = bitumen viscosity, in poise

Pen = penetration grade for 100 g, 5 sec loading, mm/10.

Equation 3 presents the in-service viscosity aging model for surface conditions. The model is a hyperbolic function and includes the effect of environment on the long-term aging. The environmental considerations enter through the use of the mean annual air temperature in the parameter A (Mirza and Witczak, 1995):

$$\log\log\left(\eta_{aged}\right) = \frac{\log\log\left(\eta_{t=0}\right) + At}{1 + Bt} \tag{4}$$

A = -0.004166 + 1.4123* C + C* log (Maat) +
   D* loglog($\eta_{t=0}$) (5)

B = 0.197725 + 0.0683841 log (C) (6)

$C = 10^{(274.4946 - 193.831\log(T_R) + 33.9366\log^2(T_R))}$ (7)

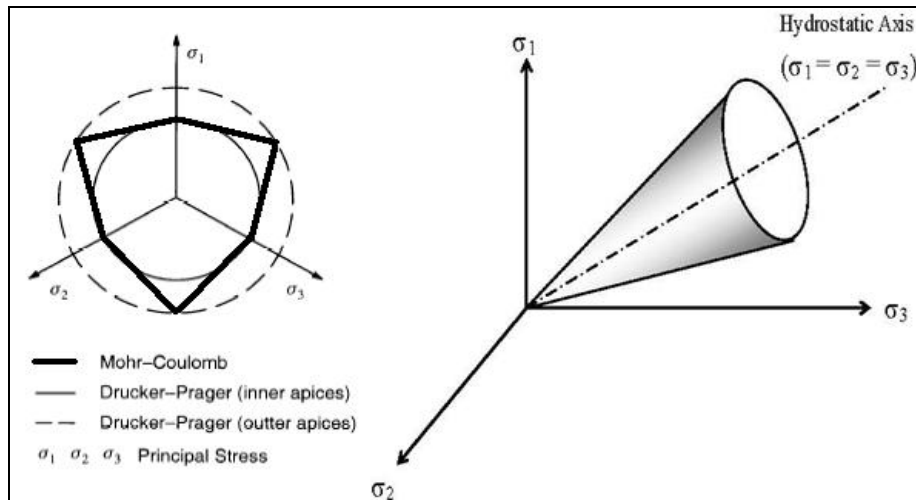D = -14.5521 + 10.47662 log(T_R) – 1.88161 log^2 (T_R) (8)

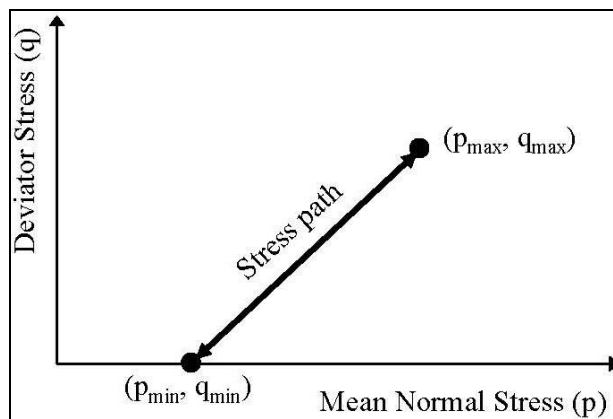**Figure 4: Drucker–Prager failure criterion**

Figure 5: The definition of a stress path in p-q stress space

η_{aged}: aged viscosity, [cP].

$\eta_{t=0}$: viscosity at mix/lay-down, [cP].

$$\log \log (\eta_{t=0}) = 0.054405 + 0.972035 \log \log (\eta) \qquad (9)$$

Maat: mean annual air temperature, [^{0}F], ^{0}F= 1.8*^{0}C+32

T_R: temperature in Rankine , [^{0}Ra] , ^{0}Ra = ^{0}F + 460

t : time in months.

Finally, the depth model describes the aged viscosity as a function of depth based on the aged viscosity from the surface aging model and viscosity at mix/lay-down. Equation 10 presents the viscosity-depth relationship (NCHRP, 2004).

$$\eta_{aged,z} = \frac{\eta_{aged}(4-\alpha) - \alpha(\eta_{t=0})(1-4z)}{4(1+\alpha z)} \qquad (10)$$

$\eta_{aged,z}$: Aged viscosity at time t and depth z, [MPoise].

η_{aged}: Aged surface viscosity, [MPoise].

z : Depth, [in]

$$\alpha = 23.83 \; e^{(-0.0308 \; \text{Maat})} \qquad (11)$$

- mean annual air temperature = 18^0 C (General Organization of Weather Observation in Syria, Data between (1980-2005)).

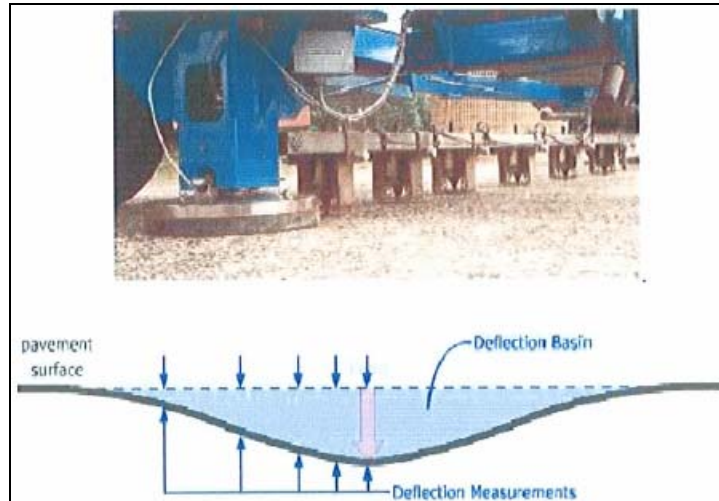- Loading time = 0.1 sec. (ASTM, 1982, 1985).

Figure 6: FWD sensors configuration and sample deflection basin

Elasto-Plasticity Performance

Some materials can carry only limited tensile stress and can undergo plastic deformation under high compressive stress. One of the most common ways of simulating such material behavior and limiting the tensile stress in finite element models is elasto-plasticity. A linear-elastic perfectly-plastic Drucker–Prager model was chosen to simulate this stress–strain behavior because of its simplicity (Drucker and Prager, 1952). This criterion can be defined as a Drucker-Prager yield surface, F_s, in a p (mean normal stress, Equation 13) *versus* q (principal stress difference, Equation 14) stress space as given by Equation 12 and shown in Figure 3 (Drucker and Prager, 1952).

$$F_s = q - p \tan \beta - d = 0 \qquad (12)$$

β = the angle of the yield surface in *p-q* stress space (Figure 3);

d = the *q*-intercept of the yield surface in *p-q* stress space (Figure 3);

p = mean normal stress, Equation 13;

q = principal stress difference, Equation14

$$p = \frac{1}{3}(\sigma_1 + \sigma_2 + \sigma_3) \qquad (13)$$

$$q = \sigma_1 - \sigma_3 \qquad (14)$$

In the principal stress space, Equation 12 represents a right-circular cone with symmetry about the hydrostatic axis (Figure 4). This cone circumscribes the outer vertices of the irregular hexagonal pyramid of the Coulomb failure surface. Unlike the Mohr-Coulomb criterion (hexagonal pyramid), the circular shape of the Drucker-Prager yield surface can be readily defined in finite element formulations, as demonstrated in Figure 4.

For a linear–elastic perfectly-plastic material, the yield surface is fixed in stress space, and therefore plastic deformation occurs only when the stress path moves on the yield surface (Figure 4). On the other hand, elastic behavior occurs if, after incremental changes of stresses, the new state of stresses is within the elastic domain, *i.e.*, if $f < 0$.

For the linear Drucker-Prager model, the ABAQUS general finite element package requires the yield surface to be defined as plotted in Figure 3. The angle of the line, β, is inputted directly, while the value of "d", the "q-intercept", is not used. Instead, a value on the yield line, σ_{0c}, is used. This value (σ_{0c}) is the yield stress where the confining stress is zero as shown in Figure 3.

The σ_{oc} required by ABAQUS is calculated using Equation 15.

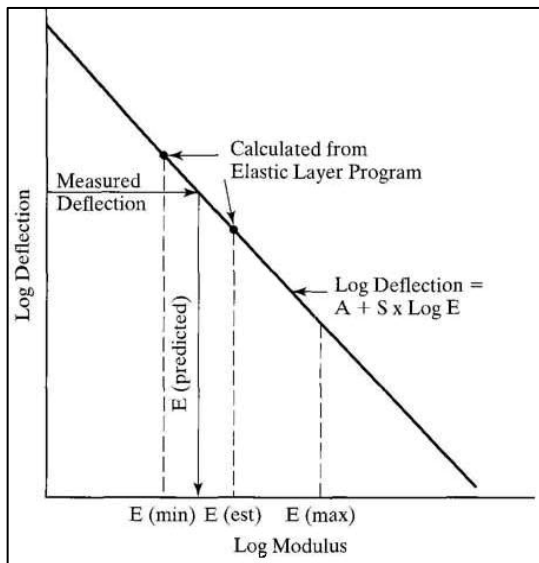$$\sigma_{oc} = \frac{d}{(1 - \frac{1}{3}tan\beta)} \qquad (15)$$

Figure 7: Relationship between deflection and modulus

If the experimental data is not readily available, the yield line can be obtained from Mohr-Coulomb friction angle, φ, and cohesion, c. From geometry, trigonometry and the relationships between *p-q* stresses and principal stresses, the Mohr-Coulomb failure line can be plotted in *p-q* space to represent a Drucker-Prager failure criterion. It can be shown that the angle of the failure line in *p-q* stress space, β, is defined by Equation 16 and the *q*-intercept, *d,* is determined using Equation 17 (Abaqus, 2009).

$$\tan \beta = \sqrt{3} \cdot \sin \varphi \qquad (16)$$

$$d = \sqrt{3} \cdot C \cdot \cos \varphi \qquad (17)$$

Similarly, σ_{0c}, required by ABAQUS is calculated using Equation 15 above.

FIELD MEASUREMENTS

To simplify and improve parameter evaluation and to complement compaction control, it is herein proposed

to take advantage of non-destructive devices that have been developed in order to perform *in-situ* measurements. Deflection testing was conducted using a Falling Weight Deflectometer (FWD). The FWD is a non-destructive testing machine, capable of imparting to the pavement surface an impulse load, similar in magnitude and duration to a moving truck wheel load. The pavement's deflections are measured using sensors, one of which is located at the center of the load plate (Figure 6). The operation is controlled by an on-board computer and the data are stored in a computer file. The sensors' spacings for this asphaltic road were 0, 200, 300, 450, 600, 900 and 1200 mm for sensors 1 thru 7, respectively.

The back calculation operation was performed using WESDEF program (Van Cauwelaert et al., 1989) which was developed by the U.S. Army Engineer Waterways Experiment Station (WES). The program is similar to the BISDEF program, which used the BISAR n-layer program (Huang, 2004).

WESDEF contains a computer optimization routine to determine a set of modulus values that provide the best fit between a measured deflection basin and the computed deflection basin when an initial estimate of the elastic modulus values and a limiting range of moduli are given. A set of *E* values is assumed, and the deflection is computed to correspond to the measured deflection. Each unknown *E* is varied individually, and a new set of deflections is computed for each variation. For each layer *i* and each sensor *j,* the intercept A_{ji} and the slope S_{ji} , as shown in Figure 7, are determined. For multiple deflections and layers, the solution is obtained by developing a set of equations that define the slope and intercept for each deflection and each unknown modulus:

$$\text{Log} (D) = A_{ji} + S_{ji} (\log E_i) \qquad (18)$$

The pavement testing was performed in the wheel path of the vehicle (i.e., about 50- 100cm from the edge of the pavement) at an average frequency of one point per kilometer, otherwise the actual location of the test
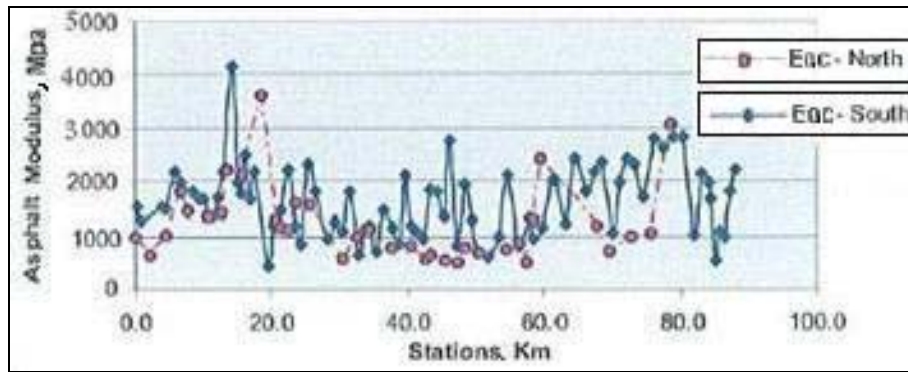
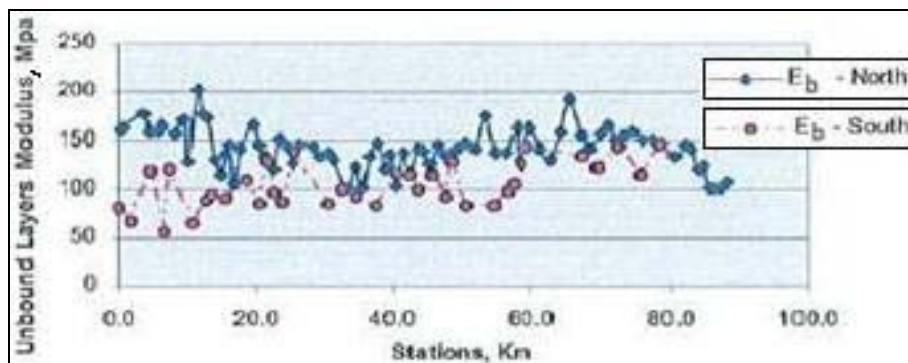**Figure 8: Asphalt layer moduli values *vs.* distance for both traffic directions**

Figure 9: Unbound layer moduli values *vs.* distance for both traffic directions
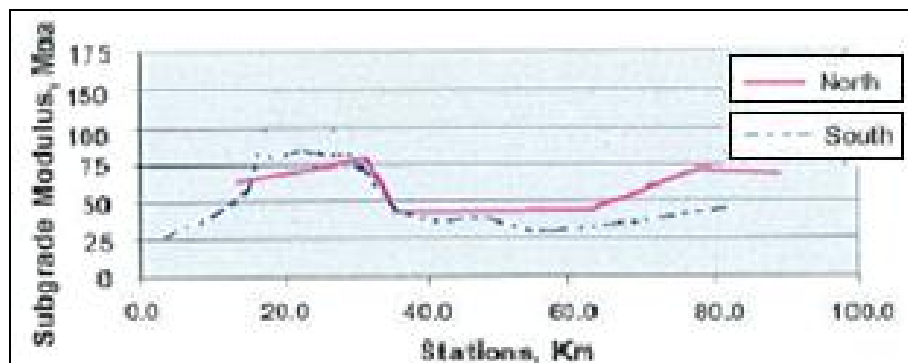

Figure 10: Subgrade moduli values *vs.* distance for both traffic directions

was controlled by the extent of severity of the pavement surface (i.e., rutting, corrugation, cracking, etc...). Two load levels were utilized at each test location corresponding as close as possible to the actual loads recorded which indicated a wheel load of about 40 kN. The pavement's back calculated moduli values are presented in Figures 8 and 9 .

The adopted procedures also permit obtaining an

estimate of the subgrade moduli values. The results are shown in Figure 10.

A field measurement is performed to determine the mean rut depth by using a 1.2 m straight edge laid across the rut and the maximum depth measured. The mean depth should be computed from measurements taken every 6 m along the length of the rut (AASHTO, 1993). The field measurement showed that the mean rut depth is 1cm.

Repeated Load

A legal axle in most states ranges from 80 kN to 90 kN (Yoder, and Witczak, 1975). In this study, a load of one set of dual tires of 40 kN is considered. It is assumed that this load is transferred to the pavement surface through a contact pressure of a single tire. As the stiffening effect of the tire wall is neglected, the tire contact pressure on the road is equal to the tire pressure (NCHRP, 2002). The uniform tire pressure is assumed to be 800 kPa, because there is a high rate of heavy trucks (about 18 %).

As a vehicle passes over the cubic element in a pavement, a stress pulse is applied to it. The stress pulses are applied repeatedly in large numbers for the duration of the life of the pavement. The magnitude of these stress pulses will vary due to the wide range of vehicle types. However, for illustrative purposes, it is assumed that each stress pulse is of the same magnitude (Arnold, Gregory Kenneth, 2004). A triangular wave with a duration of 0.1 second corresponding to an average speed of around 70 km/h (LCPC-SETRA, 1997) with a peak load of 40 kN is adopted in this study; see Figure 11. The duration time between two subsequent axles is assumed to be 0.2 second.
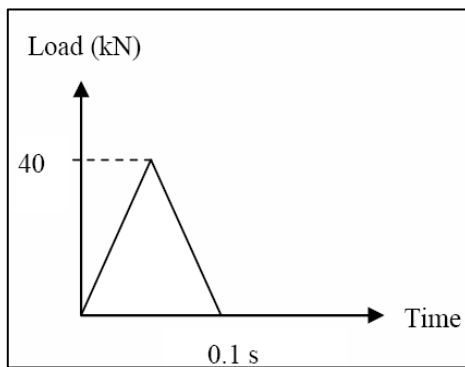

Figure 11: Load time function

Computation time for a dynamic analysis is several orders of magnitude longer than for a corresponding static calculation. There is no compelling reason for performing dynamic analysis in the 2002 Design Guide, especially given the level of idealization/approximation in the other areas of the design approach (e.g., material characterization) (NCHRP, 2004). Saad et al. (2005) compared the response of flexible pavement structures to single wheel traffic loads as a dynamic and static loading. They concluded that dynamic loading causes a response, which is represented as a rut, about 50% less than the one which the static loading generates. Green obtained the best agreement between computed and field measured deflections when the pavements were subject to static cyclic loading (Green, 2008).

Based on these considerations, and for simplicity, the load is simulated only as a static one, although in general the truck suspension system and vehicle speed do affect stresses in real pavements (Lee et al., 1993).

FINITE ELEMENT MODELING

Model Geometry

FEA has been proven suitable for application to complex pavement problems. Although using three-dimensional (3D) finite element models can solve all problems that can be solved with two-dimensional (2D) models, it is very expensive to use 3D models in terms of data preparation and computational time (Fang et al., 2004). The pavement structure has a large longitudinal dimension, which makes it suitable for using 2D plane strain models when studying transverse profiles (Fang et al., 2004). Hua compared the FEA results of pavement rutting using a plane strain model *versus* a 3D model (Hua, 2000). Figure 12 shows the predicted surface profiles of 2D and 3D models under 5000 wheel passes. It can be seen that there is no significant difference between the two models. The difference in maximum rut depths from the two models is less than 2%. Therefore, 2D plane strain models were appropriate for this study.

The mechanical (analytical) design methodology is based on predictions of pavement performance. There are many components and subsystems involved in making these predictions: inputs such as traffic loading, environmental conditions and material properties; the
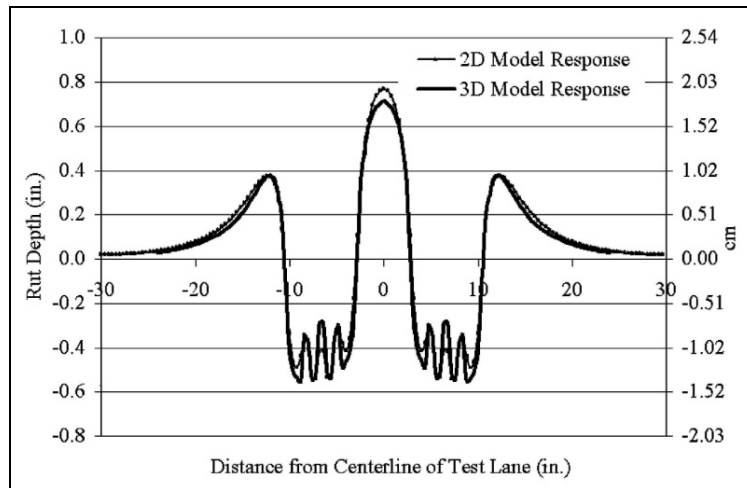
Figure 12: Comparison of 2D and 3D model responses (Hua, 2000)

Table 1: Comparisons between 2D and 3D results

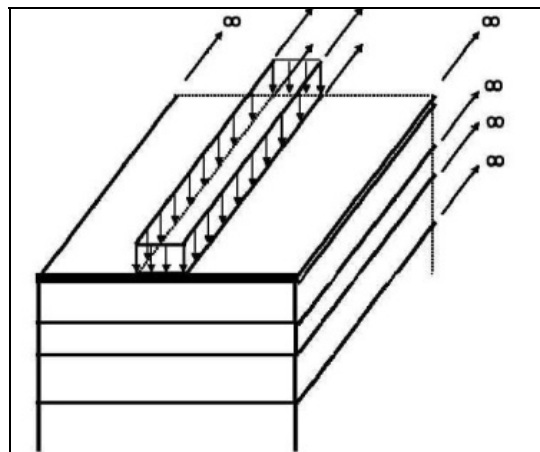| 3D		2D		Percent Difference	
Stress σ_{33} [kPa]	Strain ε_{33} x10^{-3}	Stress σ_{22} [kPa]	Strain ε_{22} x10^{-3}	σ_{33}/σ_{22} [%]	$\varepsilon_{33}/\varepsilon_{22}$ [%]
-56.486	-1.07	-53.272	-1.13	1.06	0.95

Figure 13: 2D plane strain finite element model

pavement response model; and the distress prediction model. Each of these components has an inherent inaccuracy or uncertainty. In general, the level of inaccuracy or uncertainty in the material inputs and, especially, the distress prediction model will be far greater than that of the pavement response calculations. Within this context, for example, the additional modest differences between a 2D *vs.* 3D pavement response calculation may be insignificant in practical terms (NCHRP, 2004). This point was already recognized during earlier attempts to develop the mechanical and mechanistic-empirical pavement design procedures. It is proven that the development of more sophisticated/complex/realistic structural models does

not necessarily insure 'improved' pavement design procedures. In fact, the structural model is frequently the 'most advanced' component. Inputs and transfer functions are generally the components lacking precision (Thompson, 1990). Jacobs et al. assumed a plane strain model for fracture/cracking analysis for overlay design of pavements. However, they used a 3D

model to calibrate the plane strain model where the strip loading in the 2D model was changed until the results were similar to those obtained in the 3D model (Jacobs et al., 1992). Also, Long et al. used a plane strain model (Long et al., 2002) to simulate pavements tested by the HVS (Heavy Vehicle Simulator) in a rutting study described by Harvey and Popescu (2000).
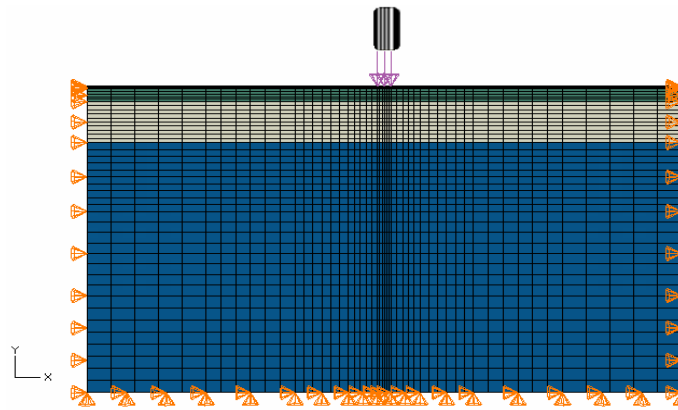

Figure 14: Model mesh and boundary conditions

Table 2: Material properties

Layers	Density (N/m^3)	Poisson's ratio v (%)	E-Modulus (Pa)	β (dgree)	Stress yield σ_{oc} (Pa)
AC	24000	0.4	1700 E^6	46.18	272940
Granular course	20000	0.35	120 E^6	48.06	44500
Subgrade	17000	0.35	50 E^6	43.00	17000

In this research, the responses analyzed with 2D and 3D simplified models are compared. The same finite element mesh, geometric characteristics, boundary conditions, material properties and loading conditions were used for all analyses in the two simplified models. The results' analysis of the principle stresses and the vertical strains at the top of the subgrade beneath tire centerline are presented in Table 1.

Plane strain model is used in this study. A plane strain model assumes that the thickness in the horizontal plane is infinite. Geometry in the horizontal plane does not change so that strain is nil. Loading is assumed as a strip extending infinitely in the horizontal plane as shown in Figure 13.

The pavement section of the studied highway is simulated by using a 2D plane strain finite element model. The model consists of an asphalt course layer with a thickness of 0.25 m and a granular course layer with a thickness of 0.80 m. Based on the assumption that there is no deformation beyond a certain depth in the subgrade (NCHRP, 2002), the depth of the subgrade was fixed at 4.95 m. A series of finite element analyses was performed with increasing the depth of the subgrade to determine this depth. The width of the model was selected to reduce any edge effect errors and when the effects of boundaries become negligible, so it was set at 10m. A commercially available finite element program, ABAQUS/Standard, was used in this study to

model the pavement structure, which has proven to be a suitable FEM program for the analysis of flexible
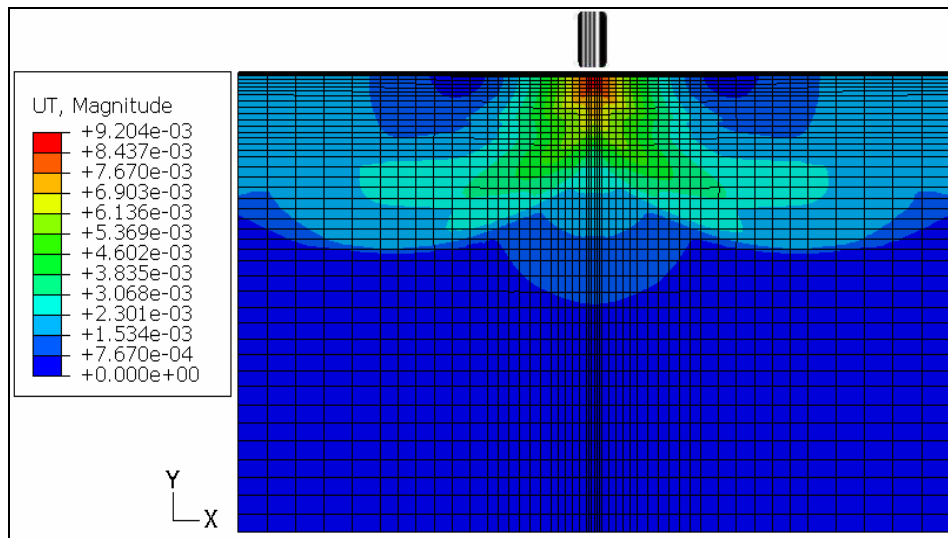
pavements (NCHRP, 2002).

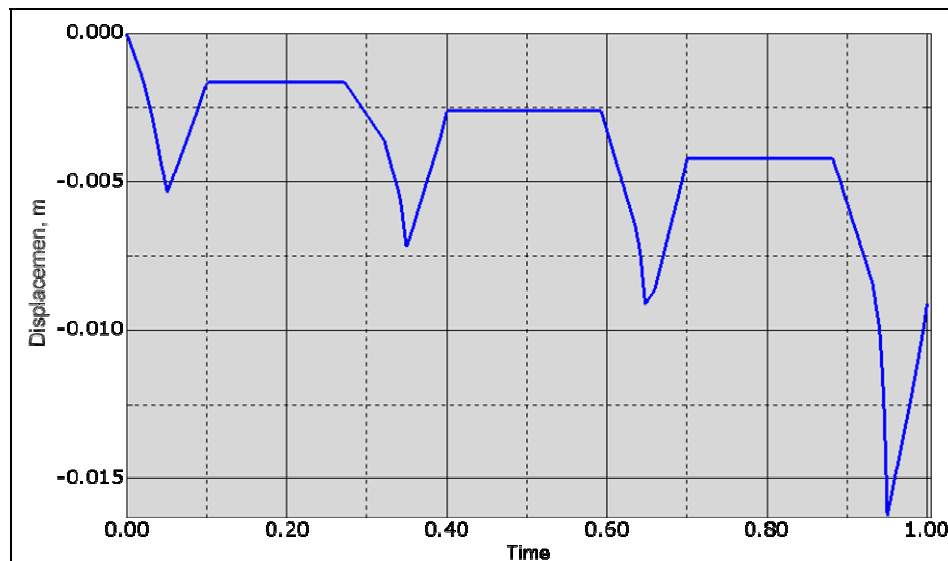**Figure 15: Contour plot of the model displacement *vs.* repeated loads**

Figure 16: The displacement curve *vs.* repeated loads in the surface point at the center of the load

Element Types and Mesh Size

The 8-node, quadrilateral plane strain element from the ABAQUS two-dimensional, solid-element library was selected for use in the analysis. All elements were 8-nodes biquadratic to improve the level of accuracy. A

series of finite element analyses was performed with decreasing the element size to determine the suitable mesh size. The mesh was a fine mesh around the loading area along the wheel path, and a relatively coarse mesh was used far away from the loading area in

vertical and horizontal directions. The total number of elements in the mesh was 2050. Figure 14 shows element types and mesh size.

Boundary Conditions

The bottom surface of the subgrade is assumed to be fixed, which means that nodes at the bottom of the subgrade cannot move horizontally or vertically. The boundary nodes along the pavement edges are horizontally constrained, but are free to move in the vertical direction. Figure 14 shows the boundary conditions.
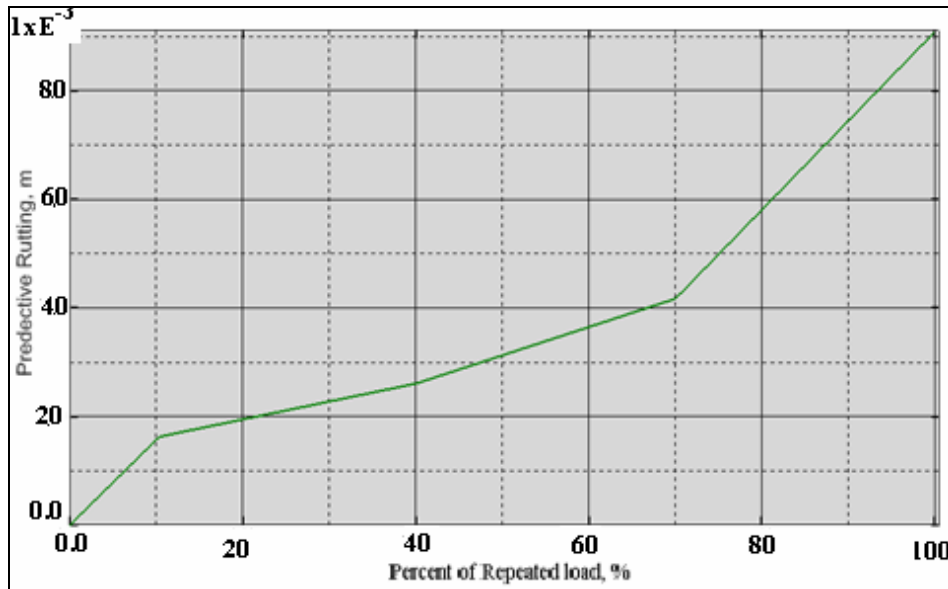

Figure 17: Predictive rutting due to repeated load

Material Characterization

Flexible pavement deformation, which occurs as a result of repeated loading, depends on the total cumulative traffic loading. In order to simulate flexible pavement deformation, a linear-elastic perfectly-plastic Drucker–Prager model is used to characterize layer materials. The complex modulus is used as a design parameter to reflect the viscoelastic characters of the asphalt paving mix. Fwa et al. (2004) presented the results of a new phase of the C– φ (cohesion and angle of friction) research program, which is aimed to develop a rutting prediction model using the C– φ concept. Employing C– φ as a failure criterion is suggested by Kim et al. (2005). They applied three analytical approaches (flow number, cohesion-friction failure and fracture energy) to determine the critical transition from soundness to unsoundness for the tested mixture.

The FWD field measurements are used to establish a benchmark for predicting pavement responses and to validate the FE model. The properties of the materials used in the analyses are summarized in Table 2.

MODEL ANALYSIS

Rutting is simulated as a vertical displacement in the model analysis. The displacement is considered as a response of applying traffic repeated loads. The final magnitude of the displacement UT beneath the center of the load at the end of loading is 0.92 cm (Figure 15). This result indicates that the predictive surface rut depth with a number of wheel loads is compared with the actual rut depth measurement, which equals 1 cm. The displacements as a result of the effect of the loading cycles at the point beneath the center of the wheel load

are illustrated in Figure 16. Particles of the pavement materials are transferred as a response of applying repeated wheel loads. A part of these displacements is recovered at the end of the load pulse, according to the resilient properties. The other part perpetuates. The permanent response is related to the plastic strains and represents the field rutting. Figure 17 shows the predictive rut depth due to repeated loads.
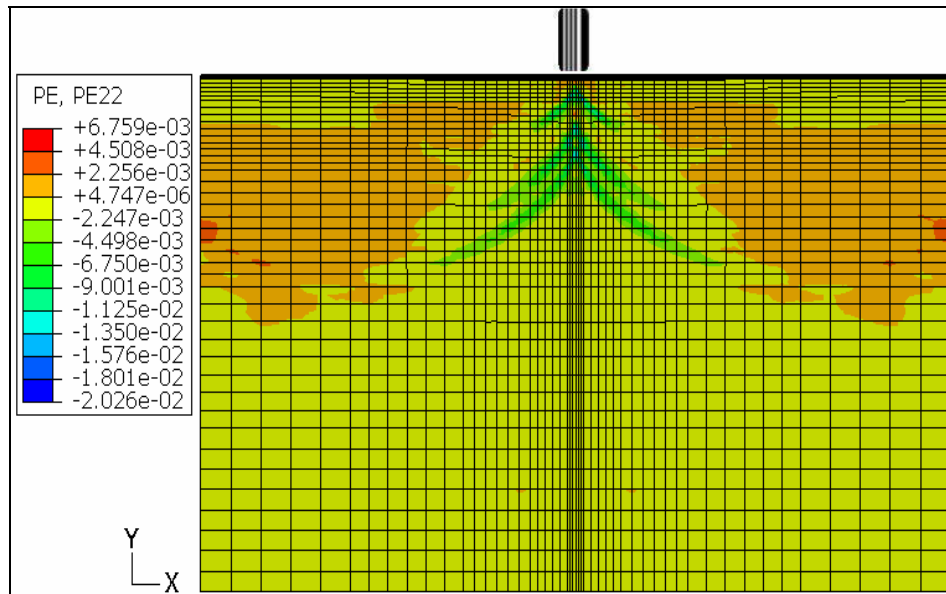

Figure 18: Contour plot of the vertical plastic strains

Figure 18 shows the vertical plastic strain distribution obtained for wheel loads. Figure 19 plots the vertical plastic strain profile *vs*. the depth from the pavement surface for the points at the center of the wheel load. Figure 20 shows the predicted surface rut profile beneath the load.

The plastic strain vanishes at 4.6 m from the surface at the centerline of the loading area. The plastic strain at the mid-depth of the AC layer is -0.00803 %, and at the mid-depth of the granular layer is -0.00799 %. Finally, the plastic strain at the mid-depth between the subgrade level and the point at which the plastic strain vanishes equals -0.00078 %.

Rut depth is obtained by applying Equation (1):

RD = 0.25* 0.00803 + 0.8* 0.00799 + 3.55* 0.000778= 0.0111 m = 1.11 cm

A comparison of prediction (1.11 cm) against field (1 cm) measurement indicates that results are close. The ABAQUS model developed in this study was considered validated for rutting prediction, which is considered a failure criterion. The model reflects the pavement performance and its response to static repeated wheel loads.

Sensitivity Analysis

The sensitivity analysis was focused on the effect of temperature on the predictive rut depth. The behavior of viscoelastic materials, such as asphalt mixtures, is strongly affected by temperature. The dynamic modulus, which was obtained using Pellinen and Witczak model, incorporated the viscoelastic behavior. In addition, the effects of tire pressure and subgrade strength on the rut depth were investigated as a pavement response.
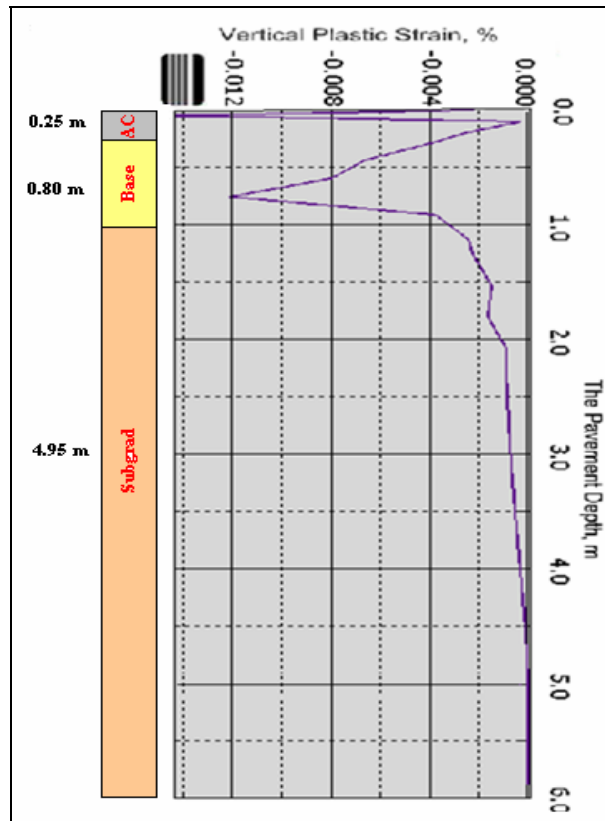
Figure 19: Vertical plastic strain profile *vs.* pavement depth
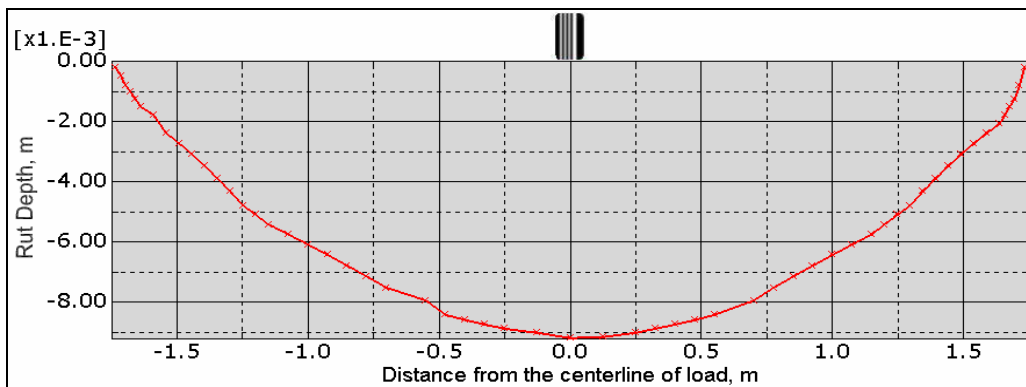
Figure 20: Predicted surface rut profile in the horizontal direction

Table 3: Temperature effect on predictive rut depth

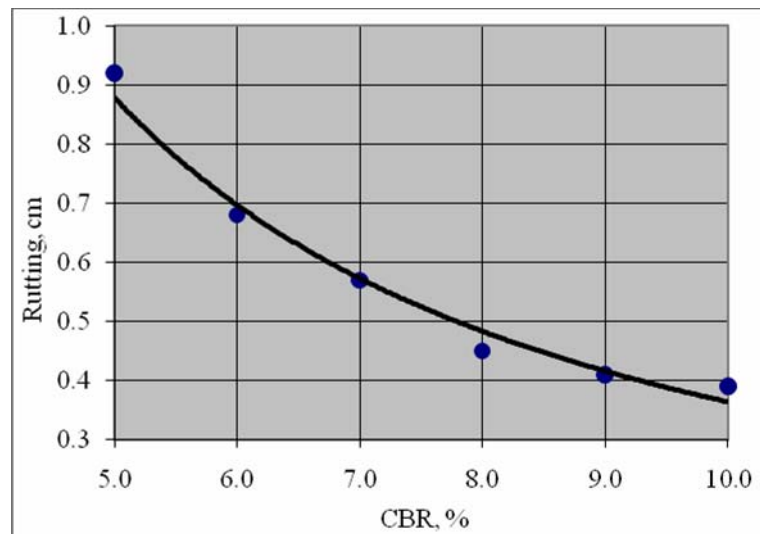| Temperature (^{0} C)	Dynamic Modulus E E* (Pa)	Internal Friction Angle β (degree)	Yield Stress σ_{oc} (Pa)	Rut Depth (cm)
40	1700 E^6	46.18	272940	0.92
25	1900 E^6	34	3910100	0.29
5	3000 E^6	15	4885600	0.18

Figure 21: The relation between CBR and predictive rut depth

Temperature Effect

The dynamic modulus is calculated according to three values of temperature (40^0, 25^0 and 5^0 C). The results were directly inputted into the developed finite element model to predict pavement response. Table 3 shows the analysis results.

Tire Pressure Effect

In order to investigate the impact of the tire pressure, three values of uniform tire pressure, of 550, 700 and 800 kPa, are assumed. The temperature is chosen to be 40^0C. Table 4 shows the analyzed predictive rut depth according to these values.

Table 4: Tire pressure effect on predictive rut depth

Tire Pressure (kPa)	Rut Depth (cm)
800	0.92
700	0.53
550	0.28

Subgrade Strength Effect

The California Bearing Ratio CBR is one of the most widely known parameters for characterizing the bearing capacity of soils and unbound granular

materials (Sweere, 1990). Empirical relationships based on CBR have been historically used for the determination of the resilient modulus of granular soils. One of these relationships is referred to in the AASHTO guide for pavement design (AASHTO, 1993).

Table 5: Subgrade strength effect on predictive rut depth

CBR (%)	M_R (MPa)	Rut Depth (cm)
5	50	0.92
6	62	0.68
7	72	0.57
8	83	0.45
9	93	0.41
10	103	0.39

$$M_R \text{ (psi)} = 1500 \text{ CBR} \qquad (19)$$

Subgrade strength evaluation is carried out in terms of CBR to analyze the impact of this parameter on the rut depth. Table 5 shows the analysis results.

CONCLUSIONS

1. Results of the developed FE models were compared with actual field measurements. It is important to emphasize that although an effort was

made to approach real pavement conditions in the developed models, based on the available laboratory results and modeling limitations, some approximations and idealizations were inevitable.

2. Several investigations have shown that the use of linear-elastic models to predict stresses and strains in pavement structures can lead to significant errors. To overcome this problem, a linear-elastic perfectly-plastic Drucker-Prager model was proposed. The analysis due this model provided acceptable results.

3. It was found that the predictive rut depth decreased by decreasing the temperature. The percentage decreases were 68.5 %, 80.4 % and 38 % due to decreasing temperature from 40^0 C to 25^0 C , from

40^0 C to 5^0 C and from 25^0 C to 5^0 C, respectively.

4. The predictive rut depth decreased by decreasing tire pressure. The percentage decreases were 42.4%, 69.5% and 47.2 % due to decreasing tire pressure from 800 kPa to 700 kPa, from 800 kPa to 550 kPa and from 700 kPa to 550 kPa, respectively.

5. The rut depth increases with decreasing the subgrade strength. The curve in Figure 21 corresponds to the relation between CBR and reduction in predictive rut depth. A power equation is available to describe this relation as shown by the following expression:

$$RD = 6.813 * (CBR)^{-1.272} \qquad (20)$$

$R = 0.977$.

REFERENCES

AASHTO. 1993. Guide for Design of Pavement Structure. Washington, D.C.: the American Association of State Highway and Transportation Officials, Part I- Chapter 1.

Abaqus, 6.9. 2009. Abaqus Theory Manual. USA: Dassault Systèmes Simulia Corp., Providence, RI.

Arnold, Gregory Kenneth. Rutting of Granular Pavements. UK, Ph.D. Dissertation, University of Nottingham, November.

ASTM. D 4123-82. 1982, 1985. Indirect Tension Test for Resilient Modulus of Bituminous Mixtures, D3497-85 Dynamic Modulus of Asphalt Mixtures. Philadelphia: American Society for Testing and Materials.

Clyne, T. et al. 2003. Dynamic and Resilient Modulus of Mn/DOT Asphalt Mixtures. Minnesota, USA: Minnesota Department of Transportation.

Dormon, G. M. 1962. The Extension to Practice of a Fundamental Procedure for the Design of Flexible Pavements. Ann Arbor, Mich., 1st International Conference on the Structural Design of Asphalt Pavements, ISAP.

Drucker, D. C. and Prager, W. 1952. Soil Mechanics and Plastic Analysis for Limit Design, *Quarterly of Applied Mathematics*, 10 (2): 157-165.

Fang, Hongbing et al. 2004. On the Characterization of Fexible Pavement Rutting Using Creep Model-based Finite Element Analysis. USA, *Elsevier, Sciencedirect: Finite Elements in Analysis and Design*, 41: 49-73.

Fwa, T. F., Tan, S. A. and Zhu, L. Y. 2004. Rutting Prediction of Asphalt Pavement Layer Using C - φ Model. USA, *Journal of Transportation Engineering, ASCE*, 675-683, September/October.

García, G. and Thompson, M. 2005. Hot Mix Asphalt (HMA) Dynamic Modulus Prediction. USA, State of the Art of Pavement Structural Design and the New AASHTO Interim Guide: CONICYT Project.

General Organization of Weather Observation in Syria. Data between (1980 - 2005).

Green, Vicki L. 2008. Investigation of Structural Responses for Flexible Pavement Sections at the Ohio-SHRP Test Road. USA, Ohio: Ohio University, Thesis of PhD.

Harvey, J. T. and Popescu, L. 2000. Rutting of Caltrans Asphalt Concrete and Asphalt-Rubber Hot Mix under Different Wheels, Tyres and Temperatures – Accelerated Pavement Testing Evaluation. Berkeley:

Pavement Research Center, Institute of Transportation Studies, University of California.

Hibbitt, Karlsson and Sorensen. 2009. ABAQUS, Finite Element Computer Program. *Theory Manual. Version 6.9-1,*. N.Y., USA, Pawtucket, RI.

Hua, J. 2000. Finite Element Modeling and Analysis of Accelerated Pavement Testing Devices and Rutting Phenomenon. Indiana, USA, Ph.D. Thesis, Purdue University, West Lafayette.

Huang, H. Yang. 2004. Pavement Analysis and Design. New Jersey: Pearson Prentice Hall, 2nd edition.

Jacobs, M. M. J. et al. 1992. Cracking in Asphalt Concrete Pavements. Nottingham, UK: 7th International Conference on the Structural Design of Asphalt Pavements, ISAP, Proc., 1: 89-105.

Kim, Sunghwan and Coree, Brian J. 2005. Evaluation of Hot Mix Asphalt Moisture Sensitivity Using the Nottingham Asphalt Test Equipment. Iowa State University: Center for Transportation Research and Education CTRE, Final Report, Project, 02-117.

LCPC-SETRA. 1997. French Design Manual for Pavement Structures. Paris: Laboratoire Central des Ponts et Chaussées and Service d'Etudes Techniques des Routes et Autoroutes.

Lee Ying Haur, Alaeddin Mohseni and Michael I. Darter. 1993. Simplified Pavement Performance Models. USA: Transportation Research Record, No. 1 397: 7- 14.

Long, F., Govindjee, S. and Monismith, C. 2002. Permanent Deformation of Asphalt Concrete Pavements: Development of a Nonlinear Viscoelastic Model for Mix Design and Analysis. Copenhagen, Denmark: 9th International Conference on the Structural Design of Asphalt Pavements, ISAP.

Mirza, M. W. and Witczak, M. W. 1995. Development of a Global Aging System for Short and Long Term Aging of Asphalt Cement. USA, *Journal of the Association of Asphalt Paving Technologists*, 64: 393-430.

NCHRP. 2004. Contributions of Pavement Structural Layers to Rutting of Hot Mix Asphalt Pavements. Washington, D.C.: National Cooperative Highway Research Program, Transportation Research Board

(TRB), National Research Council, 2002. Report 468.

NCHRP. 2004. Guide for Mechanistic-Empirical Design of New and Rehabilitated Pavement Structures. Illinois, Urbana, National Cooperative Highway Research Program, Project 1-37A. Final Report, Part 3, Design Analysis.

NCHRP. 2004. Guide for Mechanistic-Empirical Design of New and Rehabilitated Pavement Structures. Illinois, Urbana: National Cooperative Highway Research Program, Transportation Research Board (TRB), National Research Council. Final Document Appendix RR: "Finite Element Procedures For Flexible Pavement Analysis".

Pellinen, T. K. and Witczak, M. W. 2002. Stress Dependent Master Curve Construction for Dynamic (Complex) Modulus. Colorado, USA, *Journal of the Association of Asphalt Paving Technologists*, 71: 281-309.

Saad, B., Mitri, H. and Poorooshasb, H. 2005. Three-Dimensional Dynamic Analysis of Flexible Conventional Pavement Foundation. USA, *Journal of Transportation Engineering, ASCE*, 131 (6): 460-469.

Shell. 1991. The Shell Bitumen Handbook, Chapter 15 – The Mechanical Properties of Bituminous Mixes. U.K.: Shell Bitumen.

Sweere, G. T. H. 1990. Unbound Granular Bases for Roads. Delft, Netherlands: University of Delft, PhD Thesis.

Thompson, M. R. 1990. NCHRP 1-26: Calibrated Mechanistic Structural Analysis Procedures for Pavements. Washington, D.C.: National Cooperative Highway Research Program, Transportation Research Board, National Research Council, Volume I - Final Report.

Van Cauwelaert, F. J. et al. 1989. Multilayer Elastic Program for Backcalculating Layer Moduli in Pavement Evaluation. USA: American Society for Testing and Materials, STP 1026: 171-188.

Yoder, E. J. and Witczak, M. W. 1975. Principles of Pavement Design, Second Edition. New York: John Wiley and Sons, Inc.